Silica Nanoparticle Formation in the TPAOH−TEOS−H_2O System: A Population Balance Model

John L. Provis[†] and Dionisios G. Vlachos*[,‡]

Department of Chemical and Biomolecular Engineering, University of Melbourne, Victoria 3010, Australia, and Center for Catalytic Science and Technology, Department of Chemical Engineering, University of Delaware, Newark, Delaware 19716

Received: November 17, 2005; In Final Form: December 30, 2005

A model describing the kinetics of silica nanoparticle formation in the TPAOH−TEOS−H_2O system is presented. These nanoparticles are an important intermediate in the clear-solution synthesis of silicalite-1, so understanding the mechanisms by which they are formed and stabilized is a key step in determining the crystallization behavior of pure-silica zeolites. The model presented here is based on the mass-conserving form of the Becker−Döring population balance equations, describing growth and fragmentation by addition or removal of monomeric units, and modified to account for rapid equilibration of small silicate species and electrostatic and/or template stabilization of nanoparticles. The model predictions compare favorably with the experimental results. It is found that nanoparticle evolution exhibits distinct time regimes consisting of TEOS hydrolysis, condensation, nanoparticle formation, Ostwald ripening, and a self-sharpening mechanism in particle size distribution toward equilibrium due to stabilization during which no apparent changes in average particle size and pH are observed. Finally, the model provides an alternative, to a recent hypothesis, kinetics point of view to explain the enhanced stability of nanoparticles over extended periods of time.

Introduction

The chemistry of silica in alkaline solution has been studied intensively over many years[1,2] and yet remains an area in which many questions remain unanswered. Reactions involving silica and alkaline solutions control the synthesis of zeolites and sol−gel ceramics[3] and play a critical role in geological weathering processes[4] and the deterioration of Portland cements.[5] A large array of species have been shown to be formed by polymerization of small silicate units,[6] and the effect of these species on the nature of the crystalline products formed by ambient-temperature aging or hydrothermal treatment of these solutions has been hotly debated.[7−10] In particular, the exact nature of the precursor nanoparticles observed in the TPAOH−TEOS−H_2O system[11] (TPAOH: tetrapropylammonium hydroxide, TEOS: tetraethyl orthosilicate), and also more recently in systems involving cations other than TPA^+,[12,13] remains the basis of significant discussion. These nanoparticles range in size from approximately 2−10 nm, depending on synthesis conditions. Earlier reports suggested a crystalline "nanoslab" model for these particles,[8,14,15] but alternative structural models have since been shown to be more consistent with experimental data.[9,10,13,16,17] A recent review of the field of "nanozeolites"[18] provides a valuable overview of the TPAOH−TEOS−H_2O system and its relationship to other framework silicate and aluminosilicate systems.

These nanoparticles have also been shown to exhibit complex phase behavior, displaying a "critical aggregation concentration" (CAC) similar to the critical micellization concentration (CMC) observed in aqueous surfactant systems,[12] which occurs at approximately $SiO_2/OH^- \approx 1$. When silica is present below this concentration, the behavior of the solutions is dominated by small silicate species. However, when the concentration of SiO_2 is increased above the CAC, the solution undergoes an apparent phase separation into a solution still dominated by small silicate monomers and oligomers and a particulate phase. The size of these particles depends to some extent on the pH of the system, with a higher pH producing smaller nanoparticles[13,19] but is largely constant with addition of extra TEOS above the CAC.[17] The nanoparticles are comprised of a mixture of Q^2, Q^3, and Q^4 silicate sites[10] and appear to be relatively monodisperse and ellipsoidal in shape.[13] Comparison of SANS and SAXS data shows the particles to have a core−shell structure, with a core of SiO_2 surrounded by a shell of tetraalkylammonium cations.[12]

A variety of models have been presented in the literature to explain the growth of colloidal (>100 nm) silica particles via hydrolysis/condensation from a TEOS precursor. These models can generally be loosely divided into two classes: aggregative growth based on the Smoluchowski population balance[20] or growth by monomer addition.[21] Each of these classes of model can, under appropriate assumptions, explain certain aspects of the formation of silica particles with a narrow particle size distribution. However, neither model addresses the issue of the reversibility of silica polymerization, and neither has yet been applied to formation of the small nanoparticles observed in zeolite synthesis processes. A model has also been presented recently to describe the growth of silicalite-1 from these nanoparticles, assuming a mechanism based on irreversible nanoslab addition but not attempting to describe the initial formation of the nanoslabs or any issues of reversibility.[22]

Nanoparticle formation in the TPAOH−TEOS−H_2O system has been shown to be reversible,[13] and dynamic exchange of silicate monomers has been shown by two-dimensional ^{29}Si

* Corresponding author. E-mail: Vlachos@che.Udel.edu. Tel: 302-831-2830.
[†] University of Melbourne.
[‡] University of Delaware.

10.1021/jp056658m CCC: $33.50
Published on Web 02/01/2006

NMR experiments to take place in concentrated alkaline solutions.[23] It is therefore reasonable to suggest that, as a first approximation, the formation of the silica nanoparticles observed in TPAOH−TEOS−H_2O solutions will occur primarily by reversible reactions involving monomeric silicate units adding to and fragmenting from larger silicate species. The work of Klemperer and Ramamurthi[24] on the initial stages of base-catalyzed sol−gel silica polymerization also identifies the monomer rather than larger species as the primary growth unit involved in the reaction process. Upon heating, an Ostwald ripening-type process is inferred, indicative of a possible monomer-controlled addition/fragmentation mechanism.[25]

The basic aim of this work is therefore to develop a model, based on the hypothesis that addition and fragmentation of monomeric units is the controlling mechanism in silica nanoparticle formation, by which the observed behavior of the TPAOH−TEOS−H_2O system may be analyzed. Such a model must be able to describe the experimentally observed trends in system pH and particle size and give at least a qualitatively accurate description of the system evolution. The model formulation that has been selected for this purpose is a set of population balance equations based on the mass-conserving Becker−Döring model,[26] modified to account for the details of the particular system under investigation. It will be shown here that this model can predict the experimentally observed behavior of the system adequately and therefore provide valuable insight into the complex chemistry of silica in alkaline mixed-solvent environments.

Model Development

Becker−Döring Model. The Becker−Döring model, as reformulated by Penrose and Lebowitz for a constant-density (mass-conserving) system,[26] provides a good starting point for the development of an explicit model for reversible silica polymerization. This model describes the formation of clusters by the reversible combination of monomeric units, with different growth and fragmentation kernels representing different rate-controlling processes.[27,28] It has been shown that this model is readily modified to provide a description of micellization processes.[29−31] Extensive mathematical analysis has shown the formation of metastable states in both the standard and constant-density Becker−Döring models.[26,27,32] This provides further weight behind the use of this model in the analysis of silica nanoparticle formation because these particles have been shown by Monte Carlo simulations to be a metastable state in the TPAOH−TEOS−H_2O system,[33] and the approach to equilibrium at room temperature in aqueous tetraalkylammonium silicate systems has long been known to be very slow.[34] The monomer-addition model of Matsoukas and Gulari[21] may be considered to be a special case of the Becker−Döring model, neglecting fragmentation reactions. However, given that fragmentation reactions clearly play a significant role in the dynamic equilibrium present in a nanoparticle-containing silicate system, the model outlined in this work will include the full addition-fragmentation formulation of the mass-conserving Becker−Döring equations, modified for application to the case of silica nanoparticle formation.

Equations 1−3 are the standard mass-conserving formulation of the Becker−Döring model,[26] where n_i is the concentration of clusters of size i, and a_i and b_i are the forward and back rate constants, respectively, for eq 1. Note that eq 1 is presented here for neutral species only for the sake of simplicity. The actual species involved in the reactions will actually be in varying charge states as will be discussed later, but this simply involves removal of a certain number of protons from the as-written form of eq 1.

$$(\equiv\mathrm{SiOH})_i + \mathrm{Si(OH)_4} \underset{b_{i+1}}{\overset{a_i}{\rightleftharpoons}} (\equiv\mathrm{SiOH})_{i+1} + {}^3/_2\mathrm{H_2O} \quad (1)$$

$$\frac{\mathrm{d}n_1}{\mathrm{d}t} = -2a_1n_1^2 - n_1\sum_{i\geq 2} a_i n_i + 2b_2n_2 + \sum_{i\geq 2} b_{i+1}n_{i+1} \quad (2)$$

$$\frac{\mathrm{d}n_i}{\mathrm{d}t} = a_{i-1}n_1n_{i-1} - a_i n_1 n_i + b_{i+1}n_{i+1} - b_i n_i,\ i \geq 2 \quad (3)$$

TEOS Hydrolysis. Following the work of Matsoukas and Gulari,[21] TEOS hydrolysis will be treated as a single-step irreversible process with a first-order rate constant, a_0

$$\mathrm{Si(OEt)_4} + 4\mathrm{H_2O} \xrightarrow{a_0} \mathrm{Si(OH)_4} + 4\mathrm{EtOH} \quad (4)$$

Throughout the formulation of this model, n_0 represents the concentration of unhydrolyzed TEOS remaining in the system. Condensation reactions involving partially hydrolyzed TEOS will, for the sake of simplicity, be neglected. Kay and Assink[35] did develop a detailed model for acid-catalyzed hydrolysis−condensation of TMOS (tetramethyl orthosilicate) involving a full array of condensation reactions between partially hydrolyzed silicon alkoxide sites and the subsequent hydrolysis of these polymerized species. However, these reactions were taking place in a system in which hydrolysis was the rate-limiting step because of the very low levels of water (H_2O/TMOS $\approx$ 0.1−1.2) compared to the significant excess of water (H_2O/TEOS $>$ 200) in the systems of interest here. Matsoukas and Gulari [36] observed that in systems of high water content, such as those of interest here, hydrolysis is relatively fast, largely independent of water concentration, and pseudo-first-order in n_0. The reverse of the hydrolysis reaction, esterification, was observed only in systems with a significant excess of alcohol present, which is not the case here. The rate expression associated with eq 4 is therefore given by eq 5, where a_0 is the hydrolysis rate constant.

$$\frac{\mathrm{d}n_0}{\mathrm{d}t} = -a_0n_0 \quad (5)$$

The effects of ethanol generation on system development are neglected.[33]

Deprotonation Effects and pH Calculation. It is known that changes in pH have significant effects on both reaction rates and equilibrium species distributions in alkaline aqueous/ethanolic silicate solutions. It is therefore necessary to calculate both the pH and the extent of deprotonation within the system throughout the reaction process.

Here, monomeric and dimeric sites are treated individually and their known pK_a values, pK_{m1} = 9.0 and pK_{m2} = 12.6 for the first two deprotonations of the monomer ^{3} and pK_d = 9.85 for the first deprotonation of each site within the dimer (taken as the average of the first two deprotonations of a dimer, of which one will occur at each Si site),[37] are used. Higher deprotonations of these species are not considered because they are not significant in the pH range of interest. Any species larger than a dimer is treated as an "oligomeric" site, equivalent to a site within a nanoparticle. The effective pK_a of a silicon site within a large, negatively charged particle is obviously different from that of a site of the same connectivity but in less strongly charged surrounds. Rimer et al.[17] used an equilibrium-based model to describe nanoparticle formation, and fitted an effective

pK_o of 11.2 for sites within oligomers or nanoparticles. This value does not represent the actual pK_a of an isolated Q^3 site, but rather includes electrostatic effects due to negative charges within the nanoparticles.[17]

Having selected the appropriate deprotonation constants and species descriptions, the pH of the system may be calculated from electroneutrality considerations. x_j, with subscript j = m1 (singly deprotonated monomer), m2 (twice-deprotonated monomer), d (dimer), or o (oligomer/nanoparticle), represents the fraction of each silicate coordination type that is deprotonated (or twice deprotonated for m2), and H represents [H^+]. For example, x_{m2}, x_{m1}, and $(1 - x_{m2} - x_{m1})$ are the fractions of monomeric silicate that are deprotonated twice, deprotonated once, or neutral, respectively. Equation 6 gives electroneutrality, and eq 7 represents the dissociation of water. Equations 8−15 describe the deprotonation behavior of monomers, dimers, and oligomers. The oligomers (eq 14) are assumed to be essentially Q^3 sites for the sake of simplicity. TPA^+-OH^- association is neglected, interactions between TPA^+ cations and $\equiv Si-O^-$ groups have been shown not to be significant, and calculations including the effect on the equilibrium position of deviation of activity coefficients from unity have shown that the system shows close to ideal behavior.[17]

$$H + [TPA^+] = [OH^-] + x_{m1}n_1 + 2x_{m2}n_1 + 2x_d n_2 + x_o \sum_{i\geq 3} i n_i \quad (6)$$

$$H \cdot [OH^-] = 10^{-14} \quad (7)$$

Monomers:

$$Si(OH)_4 \overset{K_{m1}}{\rightleftharpoons} Si(OH)_3O^- + H^+ \quad (8)$$

$$\frac{x_{m1}H}{(1 - x_{m1} - x_{m2})} = K_{m1} \quad (9)$$

$$Si(OH)_3\,O^- \overset{K_{m2}}{\rightleftharpoons} Si(OH)_2O_2{}^{2-} + H^+ \quad (10)$$

$$\frac{x_{m2}H}{x_{m1}} = K_{m2} \quad (11)$$

Dimers:

$$-Si(OH)_3 \overset{K_d}{\rightleftharpoons} -Si(OH)_2\,O^- + H^+ \quad (12)$$

$$\frac{x_d H}{(1 - x_d)} = K_d \quad (13)$$

Oligomers/Nanoparticles:

$$\equiv SiOH \overset{K_o}{\rightleftharpoons} \equiv SiO^- + H^+ \quad (14)$$

$$\frac{x_o H}{(1 - x_o)} = K_o \quad (15)$$

Equations 6, 7, 9, 11, 13, and 15 are solved simultaneously to give the H and x_j values. These values are then used to calculate factors describing the dependence of the polymerization reaction rates on the system pH via the deprotonation states of the silicate sites to better match experimental observations of the effect of pH on nanoparticle formation.

It is known that there is an optimal pH range for the growth of large oligomers or solid phases from alkaline silicate solutions.[38] If the pH is too close to neutral, silica is relatively insoluble and the precursor species cannot form. If the pH is too high, then monomeric silicate predominates and sufficient supersaturation to cause precipitation is never attained. To reflect this fact, as well as the tendency of like-charged sites to repel each other, the Becker−Döring model has been modified. This reflects recent calculations by Mora-Fonz et al.,[39] who showed that reactions between single-charged and neutral silicate species are favored over those involving either two neutral or two charged species. Therefore, the terms f_{mj} (subscript j = m, d, or o for reactions involving monomer addition to monomers, dimers, and oligomers, respectively) are calculated by eqs 16−18 and represent the factors by which the rate expressions must be multiplied to enforce the constraint that all reactions are between a neutral site and a singly deprotonated site.

$$f_{mm} = x_{m1}(1 - x_{m1} - x_{m2}) \quad (16)$$

$$f_{md} = x_{m1}(1 - x_d) + x_d(1 - x_{m1} - x_{m2}) \quad (17)$$

$$f_{mo} = x_{m1}(1 - x_o) + x_o(1 - x_{m1} - x_{m2}) \quad (18)$$

The possibility of reactions between double-deprotonated and neutral sites was also considered by Mora-Fonz et al.,[39] who found that from a purely energetic standpoint these reactions are often highly favorable. However, it is believed to be more likely that such an encounter will result in the exchange of a proton, leaving both species in the singly deprotonated state and therefore mutually repulsive.[38] Incorporating these f_{mj} factors into the Becker−Döring model, along with the monomer source term due to TEOS hydrolysis from eq 5, gives eqs 19−21. Here, the dimer is treated separately from the larger oligomers to represent its different deprotonation tendencies.

$$\frac{dn_1}{dt} = a_0 n_0 - 2 f_{mm} a_1 n_1^2 - f_{md} a_2 n_1 n_2 - f_{mo} n_1 \sum_{i\geq 3} a_i n_i + 2b_2 n_2 + \sum_{i\geq 3} b_i n_i \quad (19)$$

$$\frac{dn_2}{dt} = f_{mm} a_1 n_1^2 - f_{md} a_2 n_1 n_2 + b_3 n_3 - b_2 n_2 \quad (20)$$

$$\frac{dn_i}{dt} = f_{mo} a_{i-1} n_1 n_{i-1} - f_{mo} a_i n_1 n_i + b_{i+1} n_{i+1} - b_i n_i,\ i \geq 3 \quad (21)$$

Equations 5 and 19−21 are solved using the GSL 1.4 implementation of the Runge−Kutta−Fehlberg 4th/5th order ODE solver with adaptive step-size control.[40]

Monomer−Dimer Equilibrium. The final modification to be made to the mass-conserving Becker−Döring model is that the equilibrium between monomeric and dimeric species is maintained throughout the reaction process. This is consistent with the experimental observation that exchange reactions between less-condensed silicate species are faster than those between more-condensed species by a factor of 10 or more.[23] This difference in time scales is significant enough that the assumption of local monomer−dimer equilibrium will hold throughout the reaction process. Maintaining the equilibrium between monomers and dimers will require the formation or breakage of only a single bond per silicate tetrahedron, whereas reactions involving addition to or fragmentation from larger

species will generally require formation or breakage of multiple bonds because the silicate sites in these species are generally Q^2 or higher. Although inclusion of this effect increases the computational complexity of the model, it is thought to be a more representative description of the system.

The equilibrium position is updated after each time step of the Runge−Kutta−Fehlberg solver, according to eqs 22−26. The terms $m_2 = x_{m2}n_1$, $m_1 = x_{m1}n_1$, $m_0 = (1 - x_{m1} - x_{m2})n_1$ represent the concentrations of double-deprotonated, single-deprotonated, and neutral monomers, respectively, and C is the total concentration of silica present as monomers and dimers. A mass balance for these species then gives

$$C = n_1 + 2n_2 = m_0 + m_1 + m_2 + 2n_2 \tag{22}$$

The deprotonation equilibria given by eqs 9 and 11, as well as the dimerization equilibrium represented by eq 24, are assumed instantaneous. The equilibrium constant, K_D, is calculated to be 63.09 from the data presented by Šefčík and McCormick.[3]

$$Si(OH)_4 + SiO(OH)_3^- \overset{K_D}{\rightleftharpoons} Si_2O_2(OH)_6^- \tag{23}$$

$$\frac{n_2}{m_0 m_1} = K_D \tag{24}$$

Combining eqs 9, 11, 22, and 24 and eliminating m_1, m_2, and n_2 gives

$$C = m_0 + \frac{K_{m1}m_0}{H} + \frac{K_{m1}K_{m2}m_0}{H^2} + 2\frac{K_{m1}K_D m_0^2}{H} \tag{25}$$

Solving this algebraically

$$m_0 = \frac{-H}{4K_{m1}K_D}\left[\left(1 + \frac{K_{m1}}{H} + \frac{K_{m1}K_{m2}}{H^2}\right) - \sqrt{\left(1 + \frac{K_m}{H} + \frac{K_{m1}K_{m2}}{H^2}\right)^2 + 4\frac{K_{m1}K_D C}{H}}\right] \tag{26}$$

m_1, m_2, and n_2 are then obtained from eqs 9, 11, and 24. Updated values of x_{m1} and x_{m2} are calculated from these concentrations for use in calculation of the f_{mj} parameters for the next model time step.

Analysis of Model Behavior. These modifications of the Becker−Döring model mean that not all of the wealth of analytical results available for long-time solutions and metastable states formed in the unperturbed system will hold exactly in this case. However, the purpose of this investigation is to provide a physically reasonable description of the system of interest rather than to produce an exhaustive mathematical analysis of its governing equations. Where results are presented with an approximate mapping to real time for comparison with experiment, a temperature of 35 °C is to be assumed. Inclusion of temperature effects is entirely feasible and will be addressed in a future communication.

Monomer/Dimer Equilibrium. The effects of the equilibrium updating procedure on the model predictions are shown in Figure 1. From this plot, it is seen that enforcing the monomer−dimer equilibrium throughout the reaction process accelerates the formation of silicate clusters significantly. Without use of the equilibrium updating procedure, that is, using eqs 5 and 19−21 only, the formation of dimers is essentially rate-limiting in the early stages of the reaction. The quadratic dependence of the rate of dimer formation on the monomer concentration, from eq 20, forces very slow dimerization in this case. Although it is likely that the actual physical behavior of the system falls somewhere between the two extremes, it is believed that the instantaneous equilibrium better captures the tendency of small silicate species to rapidly equilibrate in relatively dilute aqueous solution.

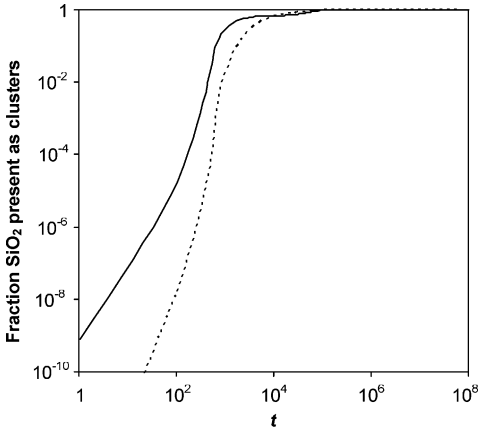

Figure 1. Effect of maintaining monomer/dimer equilibrium on the fraction of silica present as clusters ($i \geq 2$), with (solid line) and without (dashed line) monomer−dimer local equilibrium (eq 26). System composition 18TPAOH/40TEOS/9500H_2O with fast ($a_0 = a_1$) TEOS hydrolysis.

It may also be observed from Figure 1 that enforcing the monomer−dimer equilibrium at every time step has very little effect on the final state of the system. In fact, the cluster size distribution at $t = 10^8$ is essentially identical regardless of whether equilibrium is enforced. This is because the deviation from equilibrium of the small cluster sizes at long times is very small, and the medium-sized clusters comprising the bulk of the silica present are essentially in equilibrium with the monomers. Enforcing monomer−dimer equilibrium at every time step will not affect these other equilibria significantly, so the impact of the inclusion of this section of the model decreases as the reaction proceeds.

Reaction-Rate Kernel. The implementation of this model requires a choice of reaction kernel, that is, a functional form for the a_i and b_i terms. Matsoukas and Gulari [21] found that the observed particle size distribution of their silica particles was roughly consistent with a reaction-limited growth process, and this is also consistent with the observed activation energies for nucleation and growth in the clear solution synthesis of silicalite-1.[41−44] Niethammer [28] gives a brief derivation of an appropriate reaction kernel for reaction-limited growth of approximately spherical particles, the end results of which are presented as eqs 27 and 28. Here, z_s is the concentration of monomers that would be in equilibrium with an infinite flat plate as calculated from the equilibrium-based model of Rimer et al.,[17] and Γ is a parameter dependent on the surface properties of the clusters.

$$a_i = i^{2/3} \tag{27}$$

$$b_i = i^{2/3}\left(z_s + \frac{(4\pi/3)^{1/3} z_s \Gamma}{i^{2/3}}\right) \tag{28}$$

This formulation is also essentially equivalent to the kernels of Penrose[27] and of Swailes and McKee,[31] who each use a relationship of the form $b_i = a_i z_s \exp(Gi^{-1/3})$ based on chemical potential arguments. The functional form of the chosen growth and dissolution kernels is more suitable for larger clusters rather than small ones consisting of a few monomers (e.g., dimers),

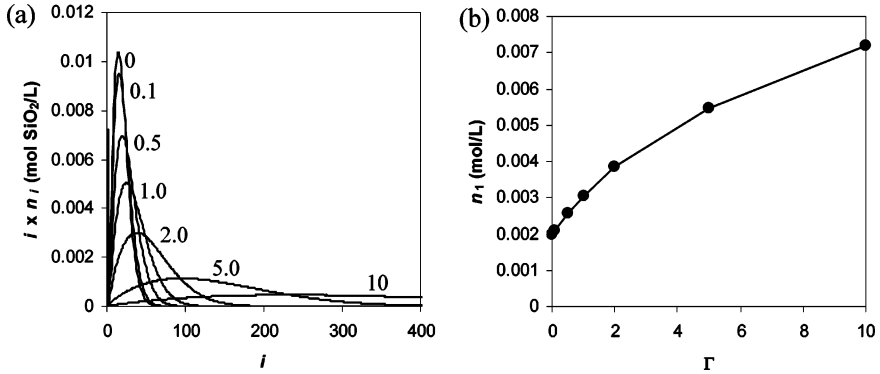

Figure 2. Effects of variations in Γ on (a) the cluster size distribution at $t = 10^7$, and (b) the monomer concentration at $t = 10^7$ for the 18TPAOH/40TEOS/9500H_2O system with fast ($a_0 = a_1$) TEOS hydrolysis.

and thus, the results should be viewed as semiquantitative in nature. Similarly, the equilibrium constants computed when using eqs 27 and 28, when the f_{mm} and f_{md} terms in eqs 19 and 20 are taken into account, are not in full agreement with the values of the equilibrium, solution chemistry model. However, given that the equilibration at every time step enforces the equilibrium literature values exactly, these small differences have a negligible effect on the model results.

In the numerical implementation of the model here, a_i and b_i values are uniformly multiplied by 10^{-3} to keep the fictive time values to a reasonable magnitude, but this is merely a matter of convenience. An approximate mapping between the fictive time and real time based on comparison of the model to nanoparticle dissolution experiments will be reported in a forthcoming publication. On the basis of this mapping, it is estimated that the time in the graphs herein should be divided by $\sim 2 \times 10^5$ to convert to real time in minutes. Work in this area is currently ongoing, and this value should be taken as being indicative only, but it does provide a preliminary means by which the model prediction may be compared to experimental nanoparticle growth data.

Figure 2 shows a comparison between the predicted particle size distributions after a set period of reaction, for different values of Γ, in the system 18TPAOH/40TEOS/9500H_2O. The period of reaction was chosen to be $t = 10^7$, where the system is evolving only gradually toward its final equilibrium state. A full analysis of the system evolution process will be presented later in this paper. However, it is sufficient at this point to note that the system is, at the time depicted in Figure 2, in a "metastable state". This is to say that for "small" clusters, that is, every cluster size smaller than a particular value determined by Γ and other system parameters, the clusters of each size are approximately in equilibrium with the monomers, and the size distribution of these clusters is therefore changing relatively slowly.[32] This slow evolution is a result of separation of time scales during nanoparticle evolution rather than a true thermodynamic metastable state, that is, a true minimum in the free energy. It thus provides an alternative "kinetics" point of view to the metastability and micellization concepts proposed earlier for explaining the long-living nanoparticles.[12,33] As will be discussed in more detail later, the larger clusters are growing at the expense of these smaller clusters, leading to a gradual shift in the monomer concentration, and therefore, changes in the positions of the pseudo-equilibria involving the smaller clusters.

The particle size distribution in Figure 2a, as well as all others presented in this work, is given as a plot of $i \times n_i$, the number of silicate sites present in clusters of size i, against i.

Figure 2a shows that a larger value of Γ gives a broader particle size distribution for the same period of reaction, centered at a larger particle size. In the vapor-condensation scenarios to which the Becker−Döring model is more commonly applied, Γ represents the destabilization of smaller particles by surface tension effects. Analogously in this system, higher values of Γ will produce systems with very strong Ostwald ripening behavior. It is seen from Figure 2b that these systems will also have a higher concentration of monomers present than if Γ is small because the equilibrium between a larger cluster and monomeric silicate species will allow for a higher concentration of monomers than would be present in equilibrium with a smaller cluster.

The interfacial energy between silica nanoparticles and the surrounding solution has been estimated by Rimer et al.[17] based on the properties of amorphous silica, but those results are unable to provide a direct prediction of Γ for use in this investigation. This parameter has therefore been set equal to 1.0 for the remainder of this study.

Figure 3 shows the evolution of the cluster size distributions for different values of the TEOS hydrolysis rate constant a_0. In all cases, hydrolysis is essentially complete at $t = 10^7$, with less than 0.02% of the TEOS remaining unhydrolyzed at this time even in the case of slow ($a_0/a_1 = 10^{-3}$) hydrolysis.

If the hydrolysis of TEOS is set to be any slower than what is shown in Figure 3a, then the reaction system takes a very long time to show significant cluster formation. Increasing the hydrolysis rate above that depicted in Figure 3d has essentially no effect on the evolution of clusters. It is seen from Figure 3, particularly by comparison of the cluster size distributions at $t = 10^6$, that slower hydrolysis produces a broader spread of sizes and larger clusters. The size distribution at $t = 10^6$ in Figure 3a peaks at a cluster size of 29, compared to 9 in Figure 3d. This is consistent with the experimental observations of Matsoukas and Gulari,[36] where slower hydrolysis rates (lower H_2O/EtOH ratios) produced larger silica particles. However, because the experiments on which this work is based are expected to fall in the fast-hydrolysis regime because of the low EtOH content of the systems, a value of $a_0/a_1 = 1.0$ has been selected for the remainder of this investigation, and growth will be reaction-limited.

The parameters used in the model are summarized in Table 1.

Analysis of Model Results

A comparison of model predictions to the experimental pH data of Fedeyko et al.[12] is presented in Figure 4. The "final"

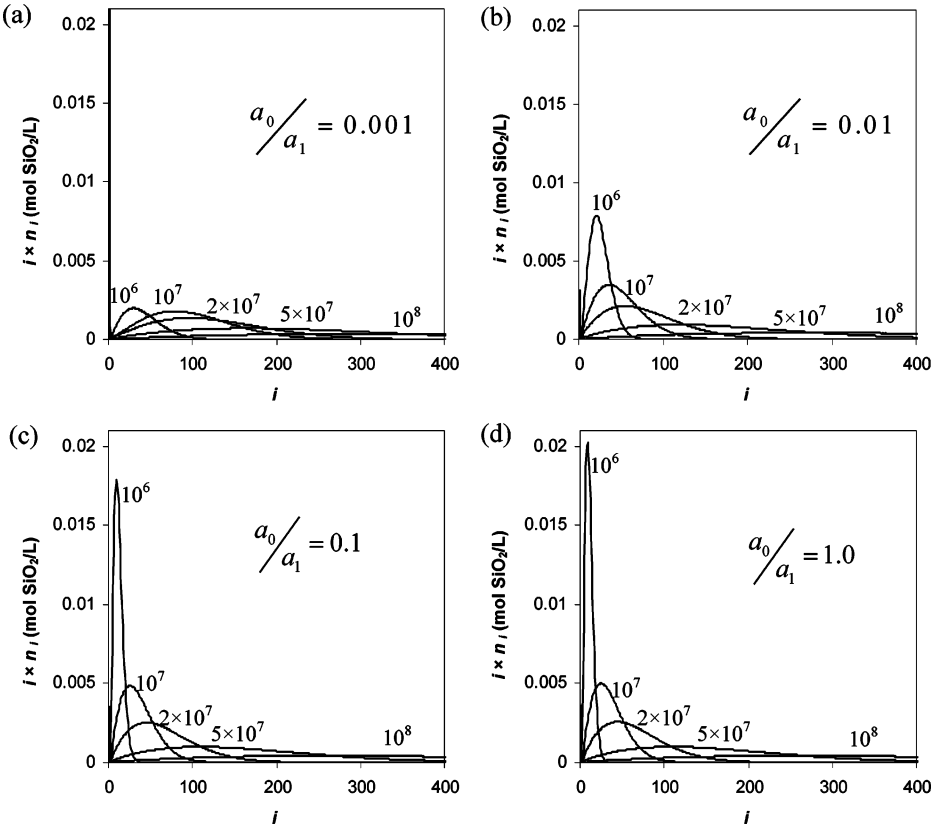

Figure 3. Cluster size distribution present after different periods of reaction (as marked on curves) with a_0/a_1 = (a) 0.001, (b) 0.01, (c) 0.1, and (d) 1.0 for the 18TPAOH/40TEOS/9500H_2O system.

TABLE 1: Model Parameter Values Used

parameter	meaning	value	reference
a_0/a_1	hydrolysis rate	1.0	
Γ	cluster surface effect	1.0	
z_s	solubility	1.05×10^{-3}	17
pK_{m1}	first monomer deprotonation	9.5	3
pK_{m2}	second monomer deprotonation	12.6	3
pK_d	dimer deprotonation	9.85	3
pK_o	oligomer/nanoparticle deprotonation	11.2	17
K_D	dimerization equilibrium	63.09	3

system pH is measured at $t = 10^7$, once hydrolysis is essentially complete and the system is evolving only slowly. The pH continues to change very slowly past this point, as discussed below. However, for the purposes of comparison with experimental data, using the model pH at this point in time is more than adequate.

From Figure 4, it is observed that the model generally predicts the experimental pH data quite well, particularly in highly alkaline systems. However, the model is in general not able to predict the sharpness of the change in system pH due to the CAC observed at $SiO_2/OH^- \approx 1.0$ for low-TPA ($x = 4$ or 9) systems. The equilibrium-based model of Rimer et al.[17] provides a somewhat better description of this phenomenon by the use of a simplified description of speciation, that is, by using a single nanoparticle of size i in equilibrium with monomers and dimers. However, their model predicts a sharper CAC than that observed in the experiments conducted at higher alkalinities. It is clear that the alkalinity changes the details of the condensation kinetics. At higher alkalinities, a population balance approach giving rise to a broader cluster size distribution better describes the data. However, the sharper transition at low alkalinity may indicate a narrower size distribution where some condensation

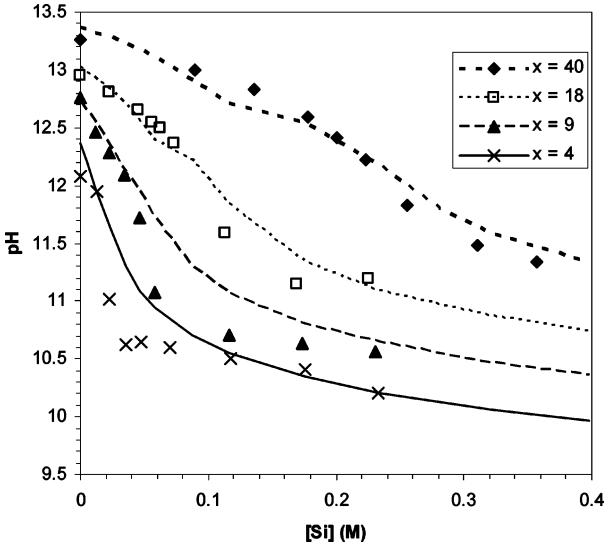

Figure 4. Comparison of the system pH predicted by the model to the experimental data of Fedeyko et al.[12] for systems of composition xTPAOH/yTEOS/9500H_2O.

between oligomeric species may occur in addition to the monomer-based processes described here because the net charge on each oligomer will be lower and therefore the repulsive forces between clusters will be lower. Such effects cannot be described by the simplified monomer-based addition/fragmentation model presented here and may therefore provide a means of explaining some of the deviations from experimental data.

Figure 5 shows the development of the cluster size distribution in the 18TPAOH/40TEOS/9500H_2O system over a very long period of reaction time. Figure 5a shows the initial stages of

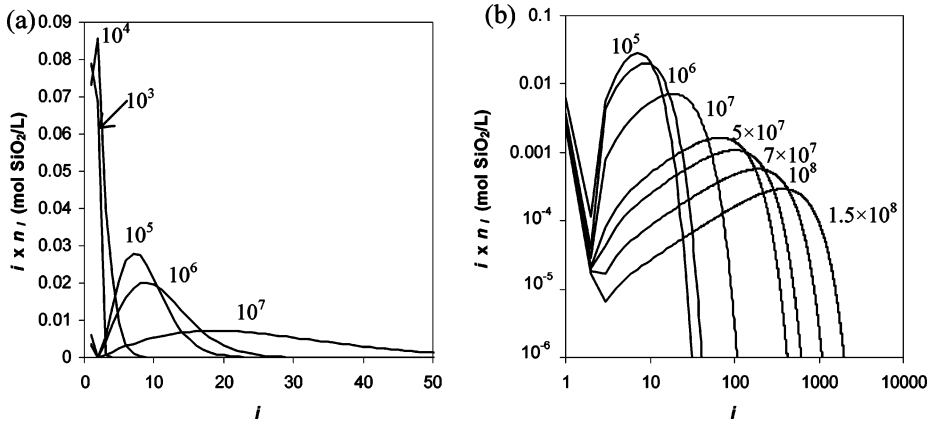

Figure 5. Development of the cluster size distribution in the 18TPAOH/40TEOS/9500H_2O system, with t values as labeled. Note the logarithmic horizontal and vertical scales in b. The longer times depicted correspond to about 12 h of real time.

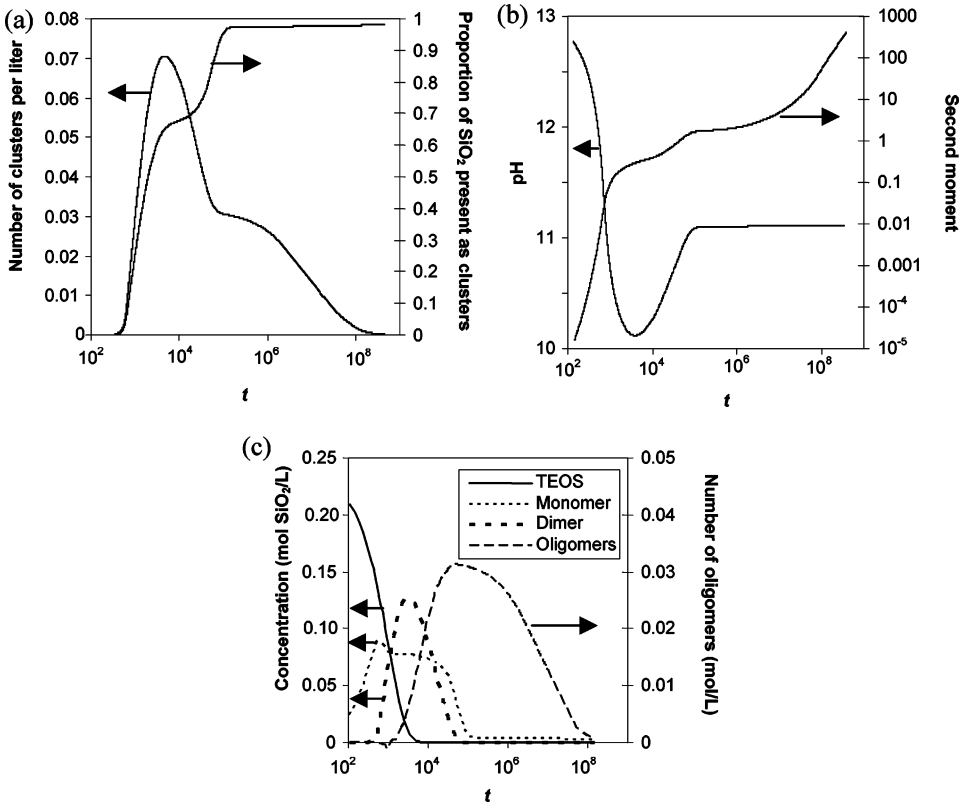

Figure 6. Time-dependent behavior of (a) the number of clusters ($i \geq 2$) per liter of solution and the proportion of SiO_2 in these clusters, (b) pH and the second moment of the cluster distribution, and (c) the concentrations (in mol SiO_2 per liter of solution) of TEOS, monomers and dimers, and the number of oligomers ($i \geq 3$) (in mol oligomers per liter), for the 18TPAOH/40TEOS/9500H_2O system. The longer times depicted correspond to about 12 h of real time.

the process, when the clusters present are generally small, and Figure 5b shows the development of much larger clusters over a prolonged period of time. Figure 6 shows the corresponding plots of the number of clusters, the fraction of SiO_2 present that is involved in these clusters, the system pH, and the second moment of the cluster distribution (proportional to an experimentally observable light-scattering signal[21]).

The behavior displayed in Figure 5 and in Figure 6 is essentially representative of that observed over the full range of compositions investigated. The rapid drop in pH in the early stages of the reaction process is due to the hydrolysis of TEOS producing relatively acidic monomeric silicate species (Figure 6c). These then dimerize, producing a sharp spike in the number of clusters (Figure 6a and c), which proceed to grow into oligomeric species at longer times. As the oligomers begin to grow, the number of clusters decreases, but their mass increases steadily and the second moment, which scales with the square of the cluster masses, increases dramatically (note the logarithmic vertical scale in Figure 6b). The pH starts to increase once the majority of the TEOS has been hydrolyzed and the monomers condense into slightly less acidic dimers and then significantly less acidic oligomeric clusters. When the majority of the silicate units are incorporated into oligomers, with only as many monomers and dimers present as are required to maintain a pseudo-equilibrium with the large clusters, the pH becomes essentially constant. It has not yet been possible to

make experimental pH measurements on a short enough time scale to determine whether this behavior is observed experimentally, but such measurements would provide valuable information regarding the relative rates of hydrolysis and condensation to either confirm or improve the assumptions used here.

Requirement for Reversible Reaction. The continuing evolution of the clusters toward an equilibrium state via an Ostwald ripening-type process is the primary difference between the predictions of this model and that of Matsoukas and Gulari.[21] In their model, which did not allow for fragmentation of clusters, the final cluster size predicted was governed to a significant extent by the initial concentration of silica. Once the supply of monomers was depleted in the irreversible model, further cluster growth was not possible. However, such dependence of the cluster size on SiO_2 concentration is not consistent with experimental data in the systems of interest here, and the absence of the Ostwald ripening processes in the irreversible model is unrepresentative of what is known to occur experimentally. Rimer et al.[17] calculated a cluster size of 356 ± 72 for the nanoparticles in 9TPAOH/*y*TEOS/9500H_2O systems using experimental data from Fedeyko et al.[13] This cluster size is relatively independent of silica concentration above the CAC at a given TPAOH/H_2O ratio but decreases with increasing TPAOH addition.[17] It is not possible to reproduce such behavior in an irreversible model. However, as is discussed below, one further simple modification to the model in the form of a cluster size cutoff factor provides a much better match of model results to experimental observations.

Nanoparticle Stabilization: Implementation of a Size Cutoff. It must be noted that Figure 5 does not show evolution of the system to a true equilibrium state. The approach to equilibrium for the reaction kernel used in Figure 5 is expected to be very slow indeed and will involve the formation of very large clusters. These very large clusters are not observed in the experimental investigation of this system, over the period of several days, but instead the metastable nanoparticles noted previously are observed. This suggests that one final modification to the model is required to capture the system behavior, involving some form of stabilization mechanism for the medium-sized ($i \approx 400$) clusters. It is not entirely clear by what mechanism these nanoparticles are stabilized, given that they have been observed in systems with a variety of different cations[13] and therefore cannot be due exclusively to TPA cation-specific effects, as has been hypothesized previously.[45] Electrostatic repulsion between the highly charged anionic nanoparticles prevents their growth by direct aggregation at room temperature, and it is likely that there is some electrostatic effect preventing, or at least greatly retarding, growth by monomer addition.[17] Much further work remains to be done in this area to resolve the true nature of these nanoparticles, to understand the mechanism by which they are formed and stabilized, and what (if any) influence they have on the final zeolitic product formed. This model provides a means by which some of the behavior of this system may be analyzed, but without having a clear quantitative understanding of the physical mechanisms governing stabilization, this effect can be described here on an empirical level only. The work of Rimer et al.[17] provides a qualitative description based on free-energy arguments, but no quantitative kinetic description is yet available.

As a means of describing nanoparticle stabilization numerically, a simple cutoff has therefore been imposed on cluster growth in the model. This is achieved by modifying the polymerization reaction kernel, eq 27, as shown in eq 29. All other components of the model are left unchanged.

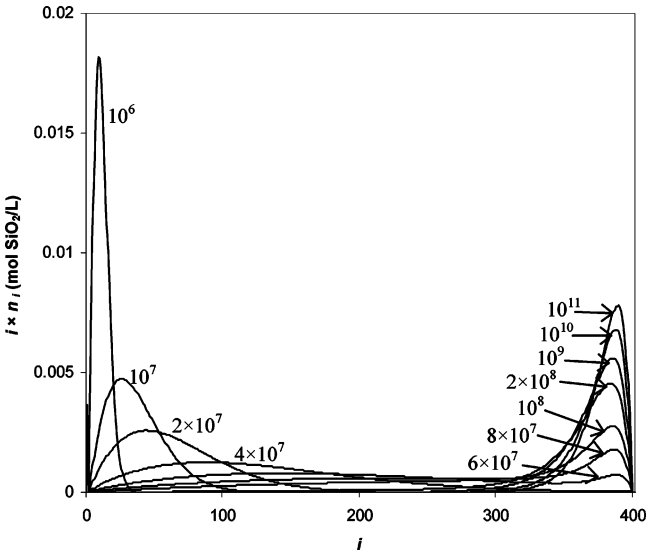

Figure 7. Development of the cluster size distribution in the 18TPAOH/40TEOS/9500H_2O system with cutoff at $i_{max} = 400$, with t values as labeled. The longer time scales range from weeks to months of real time.

$$a_i = i^{2/3}\left(1 - \frac{1}{i_{max} - i}\right) \tag{29}$$

Here, a cutoff size of $i_{max} = 400$, giving a final cluster size distribution peaked at $i \approx 390$, was chosen. The model cluster size evolution using this cutoff, which ensures that no clusters of more than 400 SiO_2 units can form, is shown in Figure 7. A sharper or broader final distribution may be obtained by manipulating the numerator of the final term in eq 29. The particular value of i_{max} appropriate for a given system will be determined in large part by the charge and template on the nanoparticles present, and the figure of 400 has been selected here for its applicability in the particular example presented below. With the availability in the future of more information regarding charge densities and the role of templates and cations in nanoparticles of different sizes under different conditions, it may be possible to extend eq 29 by use of the Poisson−Boltzmann equation to give a more fundamentally based description of this phenomenon. However, in the absence of such data, the simplest possible functional form that reproduces the experimentally observed trends has been selected for use here. Alternative functional forms can obviously be used, but the qualitative picture remains similar to what is discussed below.

It may be observed from Figure 7 that the system is still evolving toward equilibrium even after very extended periods of time ($t = 10^{11}$, a value that corresponds to about 1 year of real time). The use of a cutoff enables the numerical analysis of system evolution at much longer time scales than is computationally tractable for the unrestricted case, given that the number of ODEs that must be solved at every time step is equal to the size of the largest cluster in the system. Figure 7 shows that the change in the primary cluster size from small (<100) to large (>350) occurs relatively rapidly, and at $t \approx 4 \times 10^7$. This corresponds to the results plotted in Figure 8 detailing the evolution of this system with time. Overall, a self-sharpening mechanism of the nanoparticle size distribution is observed at long times.

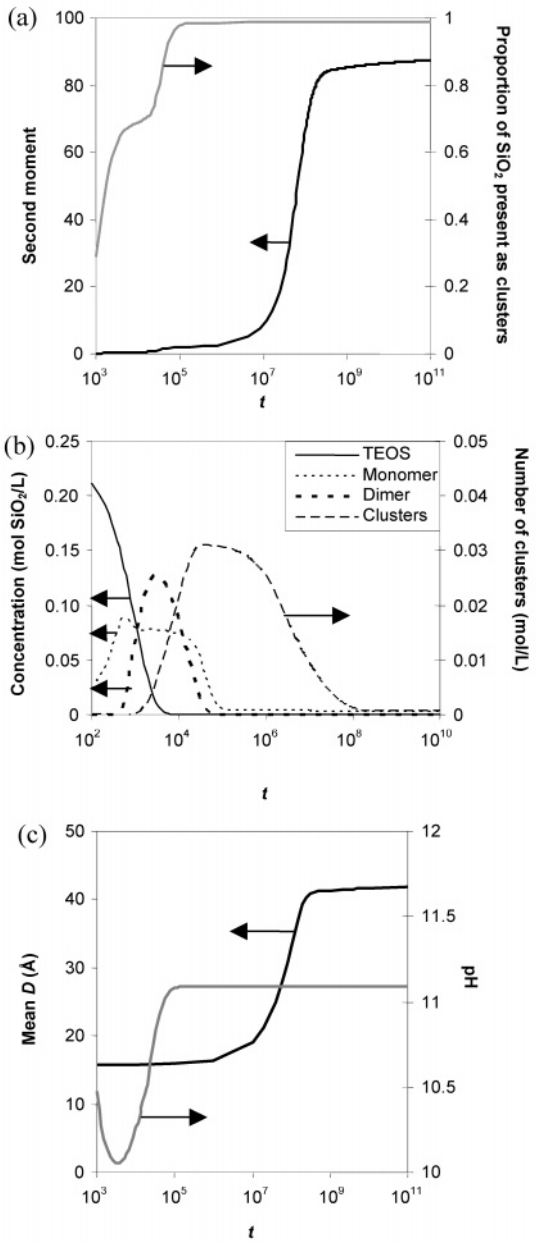

Figure 8. (a) Second moment of the cluster distribution and proportion of SiO_2 present in clusters ($i \geq 2$), (b) the concentrations (in mol SiO_2 per liter of solution) of TEOS, monomers and dimers, and the number of oligomers ($i \geq 3$) (in mol oligomers per liter), and (c) the mean diameter of clusters with $i \geq 20$ (assuming spherical particles, mass fraction SiO_2 in nanoparticles = 0.58) and pH, for the 18TPAOH/40TEOS/9500H_2O system with $i_{max} = 400$. The longer time scales range from weeks to months of real time.

It is seen that the shift from small to large clusters occurs significantly after the majority of monomeric sites have reacted to form clusters and is quite rapid. The dip in the cluster fraction curve at $t \approx 10^4$ corresponds to a dip in pH similar to that observed in the no-cutoff case in Figure 6b. Imposing the cutoff has a negligible (<0.001 units) effect on the final predicted pH at each different system composition investigated, so Figure 4 is essentially unchanged by the use of the cutoff, as shown in Figure 8c. The cutoff has only a very small effect on the concentrations of TEOS, monomers and dimers present throughout the reaction process, displayed by the fact that Figure 8b is very similar to Figure 6c. The most significant difference between these two figures is that the final number of clusters

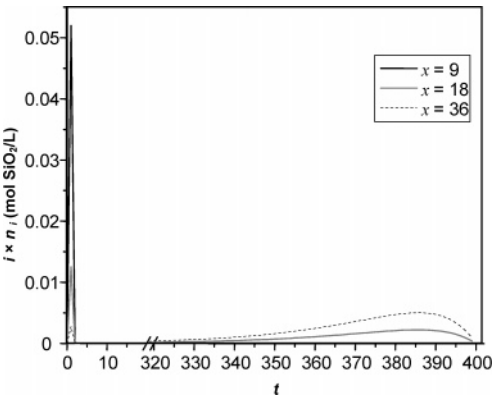

Figure 9. Comparison of the "final" ($t = 10^9$) cluster size distribution calculated with $i_{max} = 400$ for 18TPAOH/xTEOS/9500H_2O systems with silica contents below ($x = 9$, solid black line), approximately equal to ($x = 18$, solid gray line), and above ($x = 36$, dashed line) the CAC.

predicted using the cutoff is significantly higher than that predicted without this limitation because the growth to ever larger and larger clusters is restricted. The final concentration of silica nanoparticles predicted by the model with the cutoff agrees very well with experiment. Rimer et al.[25] observed that, prior to the heating experiments that were the primary focus of that investigation, the 9TPAOH/40TEOS/9500H_2O system had a nanoparticle concentration of approximately 3.2×10^{17} particles/cm^3. By comparison, the model prediction for this system with $i_{max} = 400$ is 3.3×10^{17} particles/cm^3, which matches the experimental value to within the expected error.

Figure 8c shows the evolution of the mean diameter of the clusters of size $i \geq 20$ in the 18TPAOH/40TEOS/9500H_2O system, assuming spherical clusters containing 0.58 mass fraction SiO_2 (effective core density of 1.70 g cm^{-3}).[17] During the initial period of growth ($t < 10^6$, the number of particles in the size range of interest is low, and these particles are small (Figure 7). The pH curve plotted shows that this is the time period in which the majority of the hydrolysis and small cluster formation reactions are completed. The particles then grow to close to their final size rapidly, that is, over a period of days, with a plateau in cluster size corresponding to the relatively stable long-time behavior shown in Figure 7, that is, during the self-sharpening period of several months the average particle size remains fairly constant. The overall predicted behavior is qualitatively consistent with extended experiments conducted over several months at room temperature.[48]

It may also be noted that the long-time cluster size distributions presented in Figure 7 are bimodal, consisting almost solely of monomeric silicate species in equilibrium with clusters of approximately 380−390 SiO_2 units. This correlates very well with the observations of Rimer et al.,[17] who found that an equilibrium model describing only monomers and nanoparticles provides a good fit to the experimental data in the region above the CAC. This is shown in more detail in Figure 9, which presents cluster size distributions at $t = 10^9$ for systems below, near, and above the CAC. At some intermediate times, the system is bimodal; however, the relatively low population of smaller size clusters may not be detectable with scattering techniques, especially at these time scales.

From Figure 9, it is clear that the model is able to reproduce the trends in the experimentally observed cluster size distributions. At a SiO_2 concentration significantly below the CAC, the system is predominantly monomeric, with some small oligomers also. Around the CAC, both monomers and larger

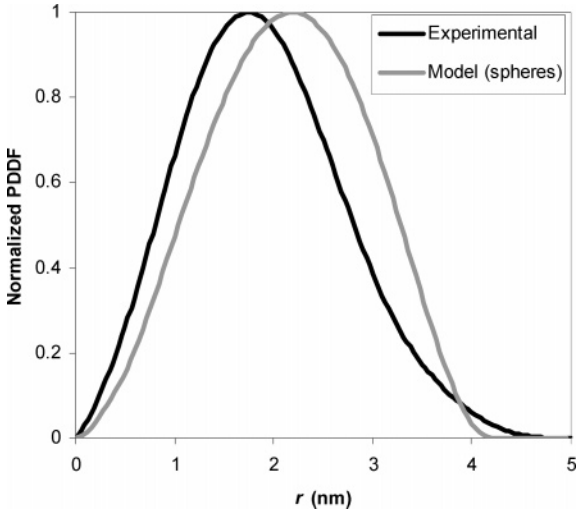

Figure 10. Comparison of model predictions to the experimental pair distance distribution function of Rimer et al.[25] for the 18TPAOH/40TEOS/9500H_2O system (model predictions assume spherical particles, mass fraction SiO_2 in nanoparticles = 0.58).

clusters are observed, and above the CAC the clusters dominate. This provides validation for the modeling approach used here, and shows that with the use of a cutoff in the form of eq 29, this model formulation provides at least a qualitatively accurate description of the speciation as the system nears equilibrium, as well as providing insight into the kinetics of this system. Clearly, a model such as this will not be uniformly applicable in all aspects of silica polymerization, particularly when growth by addition of small clusters to a crystal surface[22,46] or by aggregation of nanoparticles[20,44] is known to become the dominant mechanism.

Having calculated a "final" particle size distribution for a particular composition, direct comparison with experiment via the pair distance distribution function (PDDF)[47] is now possible. The PDDF of a dilute colloidal system represents the likelihood that two points separated by distance r fall within the same particle and can be calculated explicitly for particles of various geometries. Here, the expression for the PDDF of a set polydisperse spheres[47] (eq 30, where D_i is the number fraction of particles of size i) is used to compare the model predictions to the experimental PDDF of the 18TPAOH/40TEOS/9500H_2O system, as shown in Figure 10.

$$\mathrm{PDDF}(r) = \sum_i \left(\frac{n_i}{\sum_i n_i} \right) \cdot 12 \left(\frac{r}{D_i} \right)^2 \left(2 - 3\left(\frac{r}{D_i} \right) + \left(\frac{r}{D_i} \right)^3 \right) \quad (30)$$

Figure 10 shows that, even with the assumption of spherical nanoparticles, the calculated cluster size distribution with a cutoff of $i_{max} = 400$ provides a relatively close match to the PDDF calculated from the experimental SAXS data of Rimer et al.[25] Tuning the cutoff size could improve the agreement with the experiment, but this is not the scope of this work.

Advantages and Limitations of this Model. As a means of describing silica nanoparticle formation, this model must necessarily be compared to the lattice Monte Carlo simulations of Jorge et al.[33] and the equilibrium model of Rimer et al.[17] Clearly, a Monte Carlo simulation has the advantage of describing the system at a molecular level and can provide information about particle shape and internal structure of nanoparticles. However, the system size that can be studied by the lattice Monte Carlo method is necessarily small. As a result, it is not possible to simulate enough clusters to generate statistical information. Furthermore, information about reaction kinetics and time scales is generally lacking. Although metastability has been observed in this system, it is unclear whether this is a result of thermodynamics or the inherent inability of Monte Carlo simulation to deal with stiff systems and long time behavior. As a last note, the CPU time of our population balance approach is only hours (for treating actual concentrations) compared to many days or weeks needed for Monte Carlo simulations (for treating small size systems with a few nanoparticles).

An equilibrium-based approach provides the opportunity for further insight into the electrostatic forces acting on the nanoparticles and smaller species at equilibrium but relies on the assumption of monodisperse nanoparticles and also cannot provide kinetic information. The reaction kinetic model here must therefore be used in conjunction with these other techniques if this complex system is to be fully understood. The model presented here does not account explicitly for the effects of cations, charge stabilization, or any possible condensation between oligomers but is able to provide insight that is not available by any other technique.

Conclusions

A population balance model for silica nanoparticle formation in the TPAOH−TEOS−H_2O system has been developed. The model is based on the mass-conserving form of the Becker−Döring equations, describing growth and fragmentation by addition or loss of monomeric silicate units. The standard Becker−Döring model is modified to allow for the rapid equilibrium between silicate monomers and dimers as well as the preferential stabilization of the nanoparticles by template and/or electrostatic effects along with the solution chemistry. The form of the reaction kernel is derived from the assumption of surface reaction as the rate-limiting process. With the inclusion of a suitable cutoff function in the growth kernel, the formation of very large clusters is suppressed, corresponding to experimental results. The model provides a generally accurate description of the experimentally observed behavior of this complex system, and provides a means by which kinetic and equilibrium effects in nanoparticle formation may be analyzed. Trends in final system pH are generally reproduced satisfactorily. The bimodal (monomer−nanoparticle) cluster size distribution at SiO_2 concentrations above the CAC and the unimodal (primarily monomeric) distribution below this concentration are reproduced with a good degree of accuracy. The model provides an alternative, kinetic point of view for explaining the apparent metastability of these nanoparticles. Furthermore, it clearly shows for the first time that stabilization by template and/or electrostatic effects is a key ingredient to the stability of these nanoparticles. In the absence of such a stabilization mechanism, Ostwald ripening is relatively fast and the particle size distribution is too wide. Overall, nanoparticle evolution exhibits distinct time regimes: TEOS hydrolysis, condensation by monomer addition leading to cluster formation, Ostwald ripening by monomer dissolution from smaller clusters and addition to larger clusters, and then a self-sharpening mechanism of the particle size distribution toward equilibrium due to stabilization during which no apparent changes in average particle size and pH are observed. Finally, comparison of this model to a previous thermodynamic one, based on a monodisperse distribution, indirectly indicates that a broader cluster size distribution is most probable at higher alkalinities than at lower alkalinities.

Acknowledgment. This work was funded in part by the National Science Foundation Nanoscale Interdisciplinary Research Team (NIRT) under Grant CTS-0103010 and by an Australian-American Fulbright Postgraduate Scholarship awarded to J.L.P. that allowed him to spend some time at the University of Delaware during the Spring semester of 2005. We also thank Jeffrey Rimer and Joe Fedeyko for helpful discussions and for providing experimental data, and Prof. Scott Auerbach for providing us with a preprint of ref 33.

References and Notes

(1) Vail, J. G. *Soluble Silicates: Their Properties and Uses*; Reinhold: New York, 1952; Vol. 1.
(2) Iler, R. K. *The Chemistry of Silica: Solubility, Polymerization, Colloid and Surface Properties, and Biochemistry*; Wiley: New York, 1979.
(3) Šefčík, J.; McCormick, A. V. *AIChE J.* **1997**, *43*, 2773.
(4) Smith, J. V. *Proc. Natl. Acad. Sci. U.S.A.* **1998**, *95*, 3366.
(5) Gaboriaud, F.; Nonat, A.; Chaumont, D.; Craievich, A.; Hanquet, B. *J. Phys. Chem. B* **1999**, *103*, 2091.
(6) Swaddle, T. W.; Salerno, J.; Tregloan, P. A. *Chem. Soc. Rev.* **1994**, *23*, 319.
(7) Knight, C. T. G. *Zeolites* **1990**, *10*, 140.
(8) Kirschhock, C. E. A.; Ravishankar, R.; Verspeurt, F.; Grobet, P. J.; Jacobs, P. A.; Martens, J. A. *J. Phys. Chem. B* **1999**, *103*, 4965.
(9) Knight, C. T. G.; Kinrade, S. D. *J. Phys. Chem. B* **2002**, *106*, 3329.
(10) Kragten, D. D.; Fedeyko, J. M.; Sawant, K. R.; Rimer, J. D.; Vlachos, D. G.; Lobo, R. F.; Tsapatsis, M. *J. Phys. Chem. B* **2003**, *107*, 10006.
(11) Schoeman, B. J.; Regev, O. *Zeolites* **1996**, *17*, 447.
(12) Fedeyko, J. M.; Rimer, J. D.; Lobo, R. F.; Vlachos, D. G. *J. Phys. Chem. B* **2004**, *108*, 12271.
(13) Fedeyko, J. M.; Vlachos, D. G.; Lobo, R. F. *Langmuir* **2005**, *21*, 5197.
(14) Ravishankar, R.; Kirschhock, C. E. A.; Knops-Gerrits, P. P.; Feijen, E. J. P.; Grobet, P. J.; Vanoppen, P.; de Schryver, F. C.; Miehe, G.; Fuess, H.; Schoeman, B. J.; Jacobs, P. A.; Martens, J. A. *J. Phys. Chem. B* **1999**, *103*, 4960.
(15) Houssin, C. J. Y.; Kirschhock, C. E. A.; Magusin, P. C. M. M.; Mojet, B. L.; Grobet, P. J.; Jacobs, P. A.; Martens, J. A.; van Santen, R. A. *Phys. Chem. Chem. Phys.* **2003**, *5*, 3518.
(16) Ramanan, H.; Kokkoli, E.; Tsapatsis, M. *Angew. Chem., Int. Ed.* **2004**, *43*, 4558.
(17) Rimer, J. D.; Lobo, R. F.; Vlachos, D. G. *Langmuir* **2005**, *21*, 8960.
(18) Tosheva, L.; Valtchev, V. P. *Chem. Mater.* **2005**, *17*, 2494.
(19) Yang, S.; Navrotsky, A.; Wesolowski, D. J.; Pople, J. A. *Chem. Mater.* **2004**, *16*, 210.
(20) Bogush, G. H.; Zukoski, C. F. *J. Colloid Interface Sci.* **1991**, *142*, 19.
(21) Matsoukas, T.; Gulari, E. *J. Colloid Interface Sci.* **1989**, *132*, 13.
(22) Erdem-Şenatalar, A.; Thompson, R. W. *J. Colloid Interface Sci.* **2005**, *291*, 396.
(23) Bahlmann, E. K. F.; Harris, R. K.; Metcalfe, K.; Rockliffe, J. W.; Smith, E. G. *J. Chem. Soc.- Faraday Trans.* **1997**, *93*, 93.
(24) Klemperer, W. G.; Ramamurthi, S. D. *Mater. Res. Soc. Symp. Proc.* **1988**, *121*, 1.
(25) Rimer, J. D.; Vlachos, D. G.; Lobo, R. F. *J. Phys. Chem. B* **2005**, *109*, 12762.
(26) Penrose, O.; Lebowitz, J. L. Towards a rigorous molecular theory of metastability. In *Fluctuation Phenomena (Studies in Statistical Mechanics VII)*; Montroll, E. W., Lebowitz, J. L., Eds.; North-Holland: Amsterdam, 1979; p 293.
(27) Penrose, O. *Commun. Math. Phys.* **1989**, *124*, 515.
(28) Niethammer, B. *J. Non-Lin. Sci.* **2003**, *13*, 115.
(29) Coveney, P. V.; Wattis, J. A. D. *Proc. R. Soc. London, Ser. A* **1996**, *452*, 2079.
(30) Coveney, P. V.; Wattis, J. A. D. *J. Chem. Soc., Faraday Trans.* **1998**, *94*, 233.
(31) Swailes, D.; McKee, S. *J. Phys. A: Math. Gen.* **1992**, *25*, 6063.
(32) Carr, J.; Duncan, D. B.; Walshaw, C. H. *IMA J. Numer. Anal.* **1995**, *15*, 505.
(33) Jorge, M.; Auerbach, S. M.; Monson, P. A. *J. Am. Chem. Soc.* **2005**, *127*, 14388.
(34) Knight, C. T. G.; Kirkpatrick, R. J.; Oldfield, E. *J. Chem. Soc., Chem. Commun.* **1986**, 66.
(35) Kay, B. D.; Assink, R. A. *J. Non-Cryst. Solids* **1988**, *104*, 112.
(36) Matsoukas, T.; Gulari, E. *J. Colloid Interface Sci.* **1988**, *124*, 252.
(37) Caullet, P.; Guth, J. L. Observed and calculated silicate and aluminosilicate oligomer concentrations in alkaline aqueous solutions. In *Zeolite Synthesis*; Occelli, M. L., Robson, H. E., Eds.; American Chemical Society: Washington, D.C., 1989; p 83.
(38) Kinrade, S. D.; Swaddle, T. W. *Inorg. Chem.* **1988**, *27*, 4259.
(39) Mora-Fonz, M. J.; Catlow, C. R. A.; Lewis, D. W. *Angew. Chem., Int Ed.* **2005**, *44*, 3082.
(40) Galassi, M.; Davies, J.; Theiler, J.; Gough, B.; Jungman, G.; Booth, M.; Rossi, F. *GNU Scientific Library Reference Manual*, 2nd ed.; Network Theory Ltd.: Bristol, U.K., 2003.
(41) Cundy, C. S.; Lowe, B. M.; Sinclair, D. M. *Faraday Discuss.* **1993**, *95*, 235.
(42) Twomey, T. A. M.; Mackay, M.; Kuipers, H. C. P. E.; Thompson, R. W. *Zeolites* **1994**, *14*, 162.
(43) Watson, J. N.; Iton, L. E.; Keir, R. I.; Thomas, J. C.; Dowling, T. L.; White, J. W. *J. Phys. Chem. B* **1997**, *101*, 10094.
(44) Nikolakis, V.; Kokkoli, E.; Tirrell, M.; Tsapatsis, M.; Vlachos, D. G. *Chem. Mater.* **2000**, *12*, 845.
(45) Kinrade, S. D.; Knight, C. T. G.; Pole, D. L.; Syvitski, R. T. *Inorg. Chem.* **1998**, *37*, 4272.
(46) Chiu, M. E.; Slater, B.; Gale, J. D. *Angew. Chem., Int. Ed.* **2005**, *44*, 1213.
(47) Kratky, O.; Porod, G. *J. Colloid Sci.* **1949**, *4*, 35.
(48) Davis, T. M.; Ramanan, H.; Drews, T. O.; Penn, R. L.; Tsapatsis, M. AIChE meeting, Cincinnati, OH, Oct. 30−Nov. 4, 2005.